INTERNATIONAL JOURNAL OF HYDROGEN ENERGY 40 (2015) 4585–4596

Available online at www.sciencedirect.com

ScienceDirect

journal homepage: www.elsevier.com/locate/he

Study of $MgH_2 + NbF_5$ mixtures: Formation of $MgH_{2-x}F_x$ solid solutions and interaction with hydrogen

S.A. Pighin*, G. Urretavizcaya, F.J. Castro

Centro Atómico Bariloche (CNEA, CONICET), Instituto Balseiro (UNCuyo, CNEA), Av. Bustillo 9500, R8402AGP, S.C. de Bariloche, Río Negro, Argentina

ARTICLE INFO

Article history:
Received 21 November 2014
Received in revised form
23 January 2015
Accepted 26 January 2015
Available online 26 February 2015

Keywords:
Hydrogen storage
Magnesium hydride
Niobium fluoride
Mechanical alloying

ABSTRACT

A mixture of MgH_2 and (7 mol%) NbF_5 has been mechanically milled under *Ar* atmosphere. The evolution of the materials has been studied by *in situ* pressure monitoring, XRD, DSC, TG, TPD, SEM, and isothermal hydrogen absorption and desorption in a volumetric device. During milling, *H*-rich and *F*-rich solid solutions $MgH_{2-x}F_x$ and MgH_yF_{2-y} are produced. After 40 h of milling both solutions merge into a single one with formula $MgH_{1.60}F_{0.40}$. This solid solution is stable under a thermal treatment of 90 h at 300 °C under 6000 kPa of H_2. Hydriding and dehydriding kinetics in the as-milled and cycled materials are considerably faster than in MgH_2 milled without additive. Desorption temperature in DSC or TG is lowered 100 °C, and the material modified with NbF_5 can be hydrided in less than 4 min at $T = 250$ °C. A *H*-rich solution is formed upon rehydriding the material, showing the reversibility of the process. The kinetic improvement seems to be due to a cooperative effect between MgH_yF_{2-y} and niobium hydride, the former providing seeding crystals for MgH_2 nucleation, and the latter working as a gateway for hydrogen transfer.

Introduction

Mg and its hydride MgH_2 have been extensively studied in the last years due to their exceptional characteristics as a potential hydrogen storage system [1]. MgH_2 contains 7.6 wt.% of H_2 and *Mg* is a low-cost abundant material. However, several drawbacks still limit the widespread use of these materials. The main shortcomings are the stability of MgH_2 and the slow hydriding and dehydriding kinetics near room temperature. This last point has been addressed, and to some extent solved, by using mechanical milling techniques, both to modify the microstructure, and to incorporate additives with catalytic function [1,2]. In particular, several works have reported the substantial kinetic improvements that occur when transition metal fluorides are used as additives [3–17]. The most effective ones are NiF_2, TiF_3, VF_4, ZrF_4 and NbF_5 [3,4], the last four belonging to groups 4 and 5 of the periodic table.

When MgH_2-TmF_n (*Tm*: transition metal element) mixtures are milled, or at most after the first hydrogen desorption, MgH_2 reacts with the fluoride TmF_n producing MgF_2, H_2 and *Tm* or its hydride (depending on the nature of *Tm*). However, it is not yet completely clear if this reaction occurs during milling [5,6] or after the first hydrogen desorption [7,9,11,12,14].

* *Corresponding author.*
E-mail address: spighin@cab.cnea.gov.ar (S.A. Pighin).
http://dx.doi.org/10.1016/j.ijhydene.2015.01.153

Irrespective of this, these materials usually present greatly enhanced hydrogen absorption and desorption kinetics, though the specific cause for the catalytic effect has not been completely established up to now. Part of the catalytic effect has been attributed to the transition metal or its hydride, and part to MgF_2 or the F^- ion [3,5,7–10,18]. However, the contribution of each compound is not yet clear. As a matter of fact, it is a complex problem in which the chemical nature of the additive is not the only variable involved. Concerning *Tm* or its hydride, as suggested by Ma et al. [8], the size and distribution of the additive, and the microstructural characteristics of the material also play a significant role. They have reached this conclusion when observing that TiH_2 produced when using TiF_3 as additive gives substantially better catalytic results than TiH_2 incorporated as a direct additive. The difference has been attributed to the distinct TiH_2 distribution in each case. Similar phenomena have been reported in other papers too [7,12,13]. The transition metal alone does not explain the whole catalytic effect. In Refs. [8,19] the authors have shown that when adding $TiCl_3$ or TiF_3 to MgH_2 by the same preparation method (*i.e.* obtaining TiH_2 with similar distribution and microstructural characteristics) the kinetic improvements in the absorption and desorption of hydrogen are significantly better in the case of the fluoride. Therefore, they conclude that some role of F^- or at least of MgF_2 is to be expected. A similar conclusion is reached in Ref. [7] when the effect of adding NbF_5 has been better than that of adding *Nb*. In general, when comparing the effect of fluorides with chlorides of the same transition metal, better results are typically observed for fluorides [3,8,9].

All these results show that some advances have been made in this area, but further work is still required to completely understand the effect of transition metal fluorides in MgH_2. In this work we analyze the effect of incorporating a greater than usual amount of NbF_5 (7 mol%) as an additive to MgH_2. The goal of the study is to understand the materials evolution during milling, the role of MgF_2 and *Nb*, and the interaction of the synthesized materials with hydrogen. The use of a greater quantity of additive facilitates the task, by magnifying the signals associated with minor phases or components. This approach allow us to observe the formation of *H*-rich and *F*-rich solid solutions $MgH_{2-x}F_x$ and MgH_yF_{2-y}, respectively, and to offer a possible explanation for the kinetic improvement induced by the addition of NbF_5.

Material and methods

Materials were prepared by milling MgH_2 and 7 mol% NbF_5 up to 80 h at room temperature under 5 bar of *Ar* in a low-energy ball mill device (Uni-Ball-Mill II, Australian Scientific Instruments) with a ball to powder mass ratio equal to 50:1. Both MgH_2 and NbF_5 were obtained from Sigma–Aldrich and had a purity of 96.5% and 98%, respectively; Ar was from Air Liquide and had a purity of 99.999%. For comparison, MgH_2 without additive was also milled using the same conditions. Samples of material at intermediate stages were taken out from the milling vessel after 3, 10, 20 and 40 h for characterization. Pressure changes inside the milling vessel were measured during the synthesis to follow the evolution of the process. All the materials were manipulated within an Ar-filled UNILab-MBraun glovebox (O_2 < 1 ppm and H_2O < 1 ppm). X-Ray diffraction (XRD) was performed in a PW1710/01, Philips Electronic Instruments with monochromated Cu Kα radiation. In some cases the samples were prepared inside a sealed chamber under *Ar* atmosphere to prevent air exposure during the measurements. When precise determination of the position of diffraction peaks was needed, a low amount of silicon was added to the samples as internal standard. The crystalline phases were identified by reference to the ICDD PDF data. Rietveld refinement of the diffractograms was done using Fullprof software [20]. Thermal analysis was performed by differential scanning calorimetry (DSC) experiments (DSC 2910, TA Instruments, under 122 ml/min *Ar* flux) and thermogravimetry (TG) measurements (TGA-HP50F, TA Instruments, under 50 ml/min He flux). Both experiments were carried out under a 5 °C/min heating rate. Morphology was analyzed by scanning electron microscopy (SEM 515, Philips Electronic Instruments). The kinetic properties of hydrogen absorption and desorption were studied using a custom-made volumetric apparatus [21]. Isothermal absorption and desorption were measured at $P = 1000$ kPa and $P = 30$ kPa for $T = 250$ and 300 °C. The reported data were acquired once repeatability was achieved after one H_2 absorption and desorption cycle. Additionally, the same instrument was used to perform thermal programmed desorption (TPD) under vacuum and with a heating rate of 9 °C/min.

Results and discussion

Material evolution during synthesis

The following reactions could take place when milling MgH_2 and NbF_5:

$$\frac{5}{2}MgH_2 + NbF_5 \rightarrow \frac{5}{2}MgF_2 + NbH_2 + \frac{3}{2}H_2 \quad (1)$$

$$\frac{5}{2}MgH_2 + NbF_5 \rightarrow \frac{5}{2}MgF_2 + NbH + 2H_2 \quad (2)$$

$$\frac{5}{2}MgH_2 + NbF_5 \rightarrow \frac{5}{2}MgF_2 + Nb + \frac{5}{2}H_2. \quad (3)$$

NbH_2 denotes the fcc δ phase (fluorite structure) that comprises the *H*/*Nb* atomic ratio in the range 1.8–2.0, and *NbH* the orthorhombic β phase NbH_x with *x* in the range 0.7–1.05 [22]. These reactions are all favored under standard conditions. From the data in Refs. [22,23] the Gibbs energy changes for the as-written reactions are:

$\Delta^\circ G_1 = -888$ kJ mol^{-1}
$\Delta^\circ G_2 = -940$ kJ mol^{-1}
$\Delta^\circ G_3 = -898$ kJ mol^{-1}.

These values show that reaction (2) is the most favorable one under standard conditions. As this situation is kept even if we take into account the effect of the range of H_2 pressure covered during milling, reaction (2) is expected to happen. Moreover, the Gibbs energy values reflect that *NbH* is the equilibrium phase, being more stable than *Nb* and NbH_2.

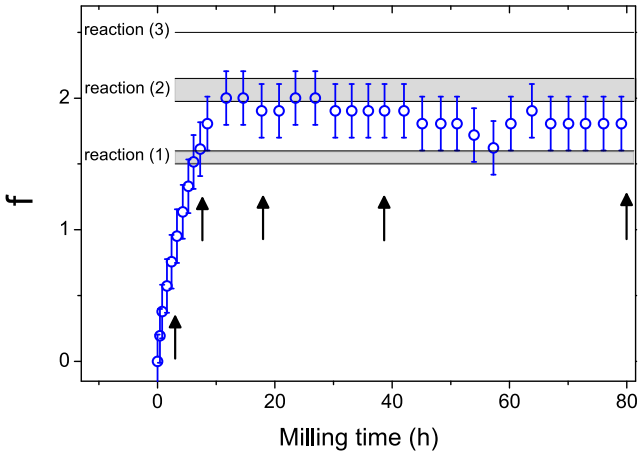

Fig. 1 – Molar ratio *f* between the released H_2 and the initial amount of NbF_5 as a function of milling time. The *f* values compatible with reactions (1–3) are also shown. The arrows indicate when samples were taken out from the milling vessel for characterization.

The evolution during milling was followed by pressure-monitoring. The molar ratio *f* between the released H_2 and the initial amount of NbF_5 was calculated from the pressure values. Fig. 1 presents the evolution of *f* with milling time. It can be seen that the reaction between MgH_2 and NbF_5 takes place without an induction period during the first 10 h of milling. After this, no H_2 is released and a constant value of *f* around 1.8 is observed. The *f* values compatible with reactions (1) and (2) are pictured in Fig. 1 as gray areas, whereas the value consistent with reaction (3) is depicted as a line. The final *f* value laying between the regions of reactions (1) and (2) suggests that more than one reaction has taken place. XRD results (discussed below) have confirmed that *NbH* and NbH_2 are present in the milled material from 10 h of milling time onwards. Therefore, reactions (1) and (2) occur during milling. The reflections of *NbH* have been clearly seen, whereas the wide peaks of NbH_2 have been identified after a Rietveld refinement of the data. The equilibrium phase has been found in greater proportion, but evidently a quantity of metastable NbH_2 was formed and remained during milling. Jin et al. [5] have identified by XRD that *NbH* appears as a consequence of milling a mixture of MgH_2 and 10 mol% NbF_5. On the other hand, Kwak et al. [6] have reported the formation of NbH_2, but when milling *Mg* and NbF_5 under 12 bar of H_2.

Fig. 2 shows images obtained by SEM of the starting MgH_2 and of samples milled 3, 10 and 80 h. The initial hydride is composed of irregularly shaped particles with sizes in the range 10–100 μm. After 3 h of milling the main morphological changes have already taken place. At this milling time the major components are agglomerates with irregular edges and characteristic sizes of approximately 5 μm. Besides, some spherical particles with diameters close to 1 μm and smooth surfaces can be found (see inset). These particles are formed as a consequence of the reaction of NbF_5 with ambient humidity during sample transfer to the microscope under air. Additionally, a few particles with the initial morphology can still be seen. For milling times longer than 3 h, the unreacted NbF_5 and the unmilled MgH_2 disappear. After 10 and 80 h of milling, the agglomerates present a very similar morphology, and the characteristic sizes are comprised in the range 0.5–10 μm, though a major proportion of bigger agglomerates can be seen in the 80 h-milled material.

The structural and chemical changes experienced by the material during milling have been analyzed by XRD measurements (Fig. 3). The most abundant phase in the 3 h-milled material is β-MgH_2 (PDF 00-012-0697). Additionally, we observe small reflections of metastable γ-MgH_2 (PDF 00-035-1184), a small peak associated with $MgNbF_7$ (due to the absence of

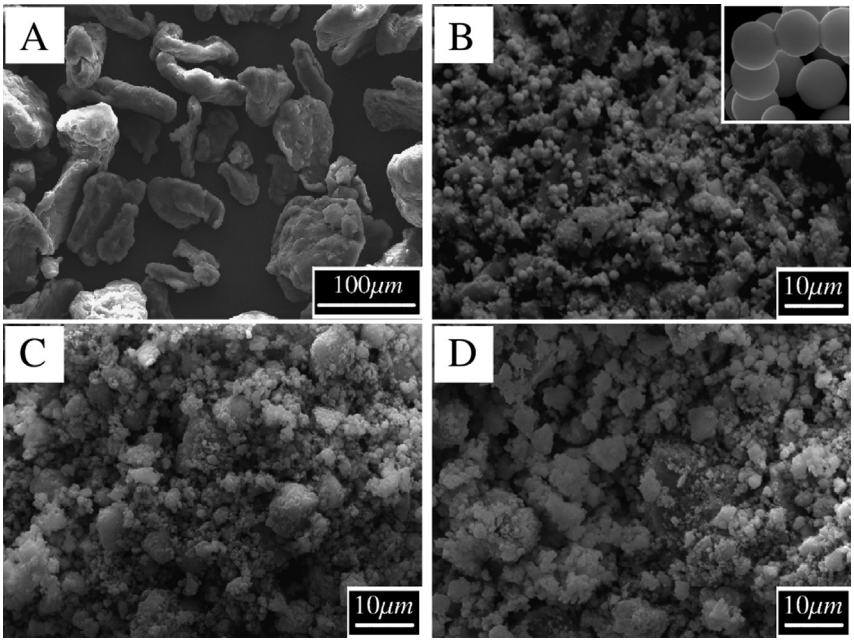

Fig. 2 – SEM images of the starting magnesium hydride (A) and the material milled 3, 10 and 80 h (B, C and D).

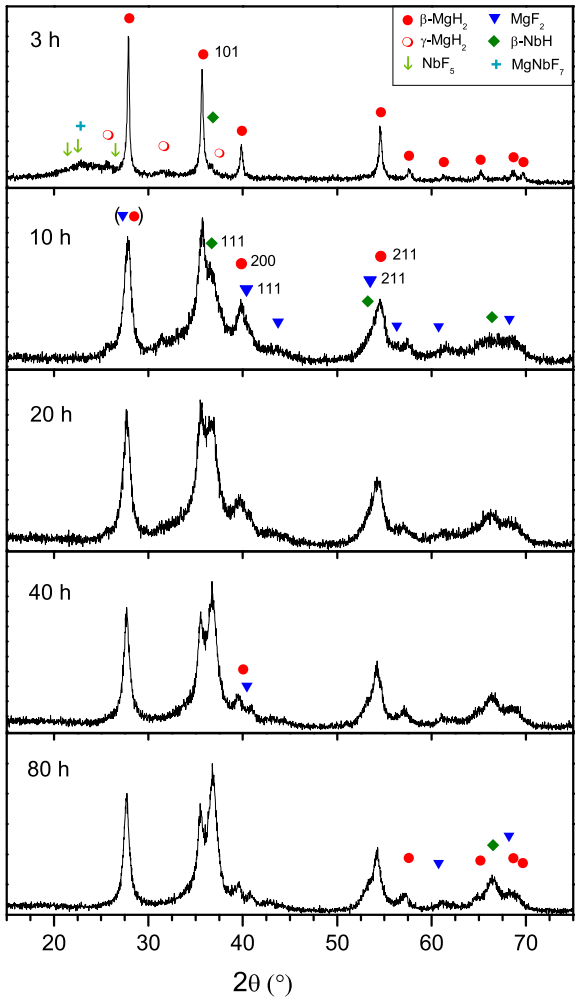

Fig. 3 – Diffractograms of as-milled samples at different milling times.

other noticeable reflections it is not possible to distinguish if it is the cubic or rhombohedral structure), a tiny reflection of *β-NbH* (PDF 00-39-1327), and an extended peak at the 2*θ* region between 20 and 26°, possibly due to an amorphous halo corresponding to NbF_5 (PDF 00-47-1230). The detection of *β-NbH* after 3 h of milling agrees with the information provided by pressure monitoring. The formation of $MgNbF_7$ as an intermediate phase has also been noted by Jin et al. [5] and attributed to a local excess of MgF_2 that limits the reaction between MgH_2 and NbF_5. The early observation of noticeable reflections of *γ-*MgH_2 after only 3 h of low-energy milling suggests a quick evolution of the material. After 10 h of milling, the low-angle reflections attributed to NbF_5 and $MgNbF_7$ disappear, *β-*MgH_2 peaks widen as a consequence of the microstructural modifications induced by milling, *γ-*MgH_2 reflections become more intense, and *β-NbH* peaks are unambiguously identified. Additionally, the MgF_2 111 and 211 reflections (PDF 00-041-1443) can be noticed as deformations of the *β-*MgH_2 200 and 211 peaks. After 20 h of milling the *γ-*MgH_2 peaks become less intense and the *β-NbH* 111 peak grows in relation to the *β-*MgH_2 101 reflection. Additionally, a slight shift of the *β-*MgH_2 peaks towards the left can be noticed. The diffractograms of the 40 and 80 h-milled materials are very similar. They present thinner peaks, a more evident increase in the *β-NbH* 111 peak intensity, and clearly resolved *β-*MgH_2 200 and MgF_2 111 peaks. It is interesting to remark two things. First, according to pressure-monitoring data the reaction between NbF_5 and MgH_2 finishes after 10 h of milling, therefore the growth of the *β-NbH* 111 peak up to 80 h is somewhat unexpected. Second, though the *β-*MgH_2 200 and MgF_2 111 peaks can be individualized, their positions are clearly shifted towards the left and the right, respectively, from the PDF card positions.

The shifts of the *β-*MgH_2 and MgF_2 XRD peaks can be better seen in Fig. 4 where a detail of the diffractograms in the 2*θ* region between 38.7 and 42° is presented. This region is particularly interesting because, despite the difficulties associated with the similarity of the diffraction patterns of the isostructural *β-*MgH_2 and MgF_2, and the considerable peak width of the milled materials, the reflections here can be undoubtedly attributed to *β-*MgH_2 or MgF_2 due to the particular intensities of these peaks (Table 1). After 3 h of milling, only the *β-*MgH_2 200 reflection can be seen. Its position coincides

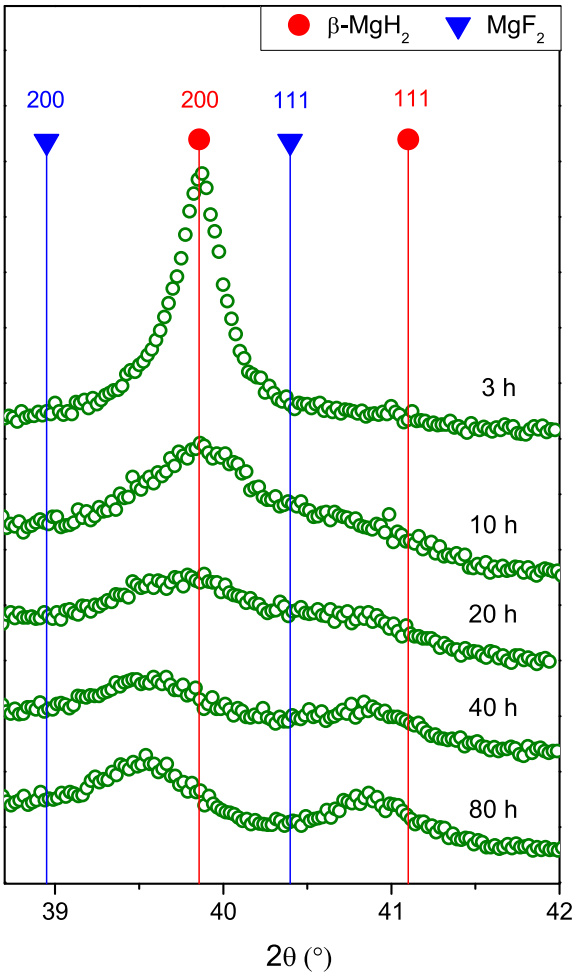

Fig. 4 – Enlarged view of the diffractograms of the as-milled samples at different milling times. Peak positions taken from PDF cards.

Table 1 – Intensities of selected XRD peaks extracted from the PDF 00-012-0697 (β-MgH_2) and 00-041-1443 (MgF_2).

Phase	hkl	2θ (°)	Intensity (%)
MgF_2	200	38.949	1
MgH_2	200	39.856	20
MgF_2	111	40.399	76
MgH_2	111	41.097	<1

with that of the PDF. After 10 h of milling a shoulder in the right side of β-MgH_2 200 corresponding to the 111 reflection of MgF_2 can be noticed. Both peaks are more or less located at the positions reported in the PDF data. With further milling, both peaks gradually shift, and after 80 h they are clearly displaced, indicating that lattice parameters have changed.

To further analyze the data we have performed Rietveld refinements of the diffractograms. The phases included and the main results are summarized in Tables 3 and 4. As the changes in lattice parameters could be a consequence of the formation of a *H*-rich solid solution $MgH_{2-x}F_x$ and a *F*-rich solid solution MgH_yF_{2-y}, these phases have been included in the refinement instead of the β-MgH_2 and MgF_2 rutile-type structures. In both cases space group $P4_2/mnm$ (136) has been kept, and the Wyckoff 4*f* positions, occupied by H^- and F^- in β-MgH_2 and MgF_2 respectively, were randomly occupied in the solutions by a refined amount of H^- and F^-. In the particular case of the 3 h-milled material, the only reliable information that could be extracted were the lattice parameters and the microstructural characteristics of the most abundant *H*-rich phase. Fig. 5 shows the evolution of the refined lattice parameters with milling time. It can be seen that the *a* and *c* values of MgH_2 and MgF_2 gradually move from the values reported in the PDF data (solid lines) to a single common pair of lattice parameters. The movement is a consequence of the gradual replacement of H^- by F^- in the initial MgH_2 and by the substitution of F^- by H^- in the synthesized MgH_yF_{2-y} solution, as the occupancy of the 4*f* site shows. After 40 h of milling the lattice parameters of *H* and *F*-rich solutions coincide within the error of the refinement. If both solutions are replaced by a single one, the refinement improves. The composition of the single solid solution after 80 h of milling deduced from the occupancy of the Wyckoff 4*f* site is $MgH_{1.60}F_{0.40}$, in excellent agreement with the formula $MgH_{1.62}F_{0.38}$ calculated from the starting amounts of MgH_2 and NbF_5 used for milling, assuming that all the F^- originally contained in NbF_5 has substituted the H^- in the initial MgH_2. Hence, by milling MgH_2 and NbF_5, $MgH_{2-x}F_x$ and MgH_yF_{2-y} solid solutions with different *x* and *y* values form for milling times up to 20 h. After 40 h of milling, both solutions merge into a single one with formula $MgH_{1.60}F_{0.40}$. In this light, the intensity changes between the β-*NbH* 111 peak and the initially supposed β-MgH_2 101 reflection can be understood as the consequence of the changes in the structure factor of β-MgH_2. As H^- is gradually being replaced by F^- the intensity of the 101 peak diminishes due to the partially destructive interference of the X-rays scattered by Mg^{2+} and F^-. We have also found that δ-NbH_2 and *MgO* are also present in the material. The appearance of δ-NbH_2 after 10 h of milling is in agreement with the pressure-monitoring data, as commented above. The presence of *MgO* is due to residual gas contamination and the high affinity of MgH_2 to H_2O and O_2.

The evolution of crystallite size and microstrain data (Table 2) shows that microstructure mainly changes during the first milling hours. The crystallite size of the starting MgH_2 decreases from 130 to 34 nm after just 3 h of milling. During this period MgH_2 starts incorporating F^- to form the *H*-rich $MgH_{2-x}F_x$. After 10 h, crystallite size diminishes to 9 nm, and remains around this value with subsequent milling. The *F*-rich crystallites are formed with sizes of 5 nm, and roughly maintain this value before merging with the *H*-rich solution to form $MgH_{1.60}F_{0.40}$. This last phase inherits the crystallite size of the *H*-rich solution. Microstrain values slightly increase with milling time when both solutions remain separated. After the merging, a decrease can be observed after 40 h of milling that slightly continues after 80 h. A similar tendency in crystallite size and microstrain is observed for β-*NbH*.

Regarding its stability, the compound $MgH_{1.60}F_{0.40}$ is not decomposed after a heat treatment of 90 h at 300 °C under 6000 kPa of H_2 (Fig. 6). Only thinner peaks due to recrystallization are observed, showing that the compound is stable in the conditions of the treatment.

Somehow, the formation of a solution $MgH_{2-x}F_x$ during the mechanical processing of these materials might be expected. MgH_2 and MgF_2 are isostructural compounds, with very close lattice parameters ($a = 4.517$ Å, $c = 3.0205$ Å and $a = 4.6200$ Å, $c = 3.0509$ Å, respectively), and mechanical milling is a technique that enhances solubility [24]. Results compatible with the formation of *Mg-H-F* solutions have been previously reported. Jin et al. [5] have observed by TEM/EDS fluorine atoms uniformly distributed inside MgH_2 grains, though they have considered premature to interpret this as evidence of F^- solution into MgH_2; Kim et al. [15] have detected *F* dissolved into MgH_2 by EDS; and Mulder et al. [14] have noticed that *F* is dissolved into *Mg* and suggested that when this *Mg* is

Table 2 – Crystallite size and microstrain of the as-milled materials from Rietveld refinement of the data.

Milling time (h)	Crystallite size (nm)				Microstrain (%)			
	$MgH_{2-x}F_x$	MgH_yF_{2-y}	$MgH_{1.6}F_{0.4}$	β-*NbH*	$MgH_{2-x}F_x$	MgH_yF_{2-y}	$MgH_{1.6}F_{0.4}$	β-*NbH*
0	130[a]	–	–	–	–	–	–	–
3	34	–	–	18	21	–	–	–
10	9	5	–	4	58	22	–	28
20	9	5	–	6	78	48	–	74
40	–	–	8	7	–	–	41	52
80	–	–	8	7	–	–	30	51

[a] This value corresponds to β-MgH_2.

Table 3 – Goodness-of-fit parameters and phases abundance (wt.%) from Rietveld refinement of the diffractograms of the as-milled materials.

Milling time (h)	χ^2	γ-MgH_2	$MgH_{2-x}F_x$	MgH_yF_{2-y}	$MgH_{1.6}F_{0.4}$	β-NbH	δ-NbH_2	MgO
10	1.4	8	48	22	–	6	6	10
20	1.8	4	52	20	–	9	6	9
40	1.8	–	–	–	77	12	5	6
80	1.7	–	–	–	78	13	4	5

Table 4 – Composition and lattice parameters of the solid solutions from Rietveld refinement of the diffractograms of the as-milled materials. The number between parentheses is the error in the last digit.

Milling time (h)	$MgH_{2-x}F_x$			MgH_yF_{2-y}			MgH_zF_{2-z} (single phase)		
	2 – x	a	c	2 – y	a	c	2 – z	a	c
3	1.96 (3)	4.517 (1)	3.020 (1)	2	4.621[a]	3.051[a]	–	–	–
10	1.97 (5)	4.524 (1)	3.019 (1)	1.4 (2)	4.613 (6)	3.045 (6)	–	–	–
20	1.89 (8)	4.531 (2)	3.021 (2)	1.4 (5)	4.60 (1)	3.04 (1)	–	–	–
40	–	–	–	–	–	–	1.65 (3)	4.549 (1)	3.029 (1)
80	–	–	–	–	–	–	1.60 (3)	4.551 (1)	3.033 (1)

[a] Not refined, the value reported for MgF_2 (PDF 00-041-1443) was used.

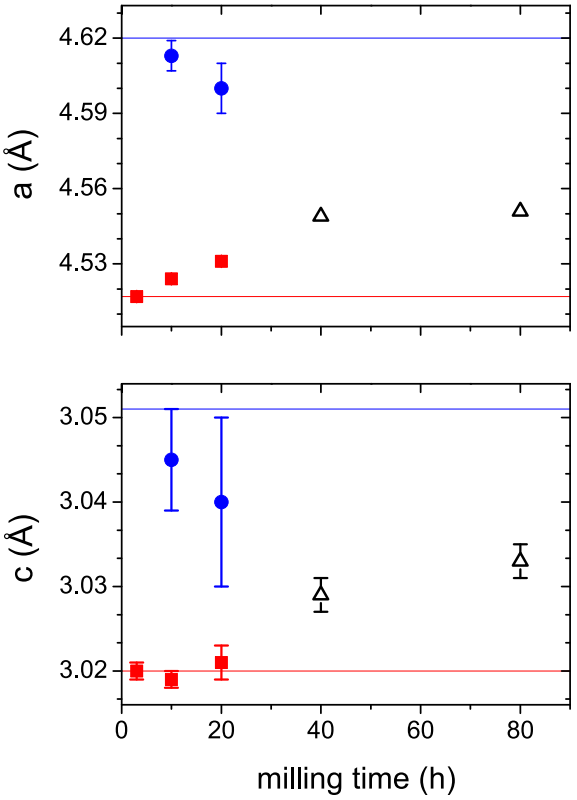

Fig. 5 – Lattice parameters of the H-rich (red squares) and F-rich (blue circles) solid solutions. Open black triangles indicate the lattice parameters obtained when refining the data with a single solid solution. Red and blue lines are the lattice parameters of β-MgH_2 and MgF_2, respectively, reported in the PDF data. (For interpretation of the references to color in this figure legend, the reader is referred to the web version of this article.)

deuterated the fluorine stays dissolved into MgD_2. The formation of a solution MgH_yF_{2-y} could also be an explanation for the unknown binding state identified by XPS measurements by Ma et al. [8] and for the shift in the F 1s peak of MgF_2 observed between the as-milled and the dehydrided state by Luo et al. [7]. In their work, Ma et al. have found that the F 1s binding energy of MgF_2 formed by milling MgH_2 and TiF_3 is approximately 0.9 eV higher than the binding energy of a reference MgF_2. They have tentatively interpreted their result as due to the formation of a ternary Mg–Ti–F compound, but in view of these results it could also be interpreted as the consequence of the solution of H^- into MgF_2. Luo et al. have observed an energy shift between the F 1s peak of MgF_2 of the as-milled material and the dehydrided sample. They have attributed the shift to defects and strain, but it could also be due to the presence of H^- ions in MgF_2. On the other hand, a coupled *ab initio*/CALPHAD study of the MgH_2–MgF_2 has been performed by Baricco et al. at 298 K [25]. Based on it, they

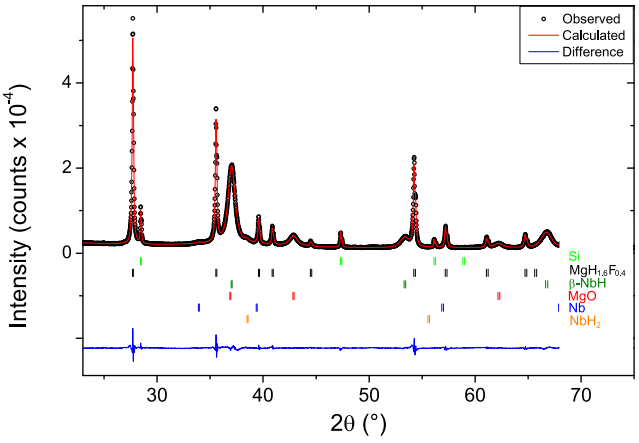

Fig. 6 – Rietveld refinement of the 80 h-milled material after a thermal treatment of 90 h at 300 °C under 6000 kPa of H_2.

predicted no F solubility into MgH_2 rich mixtures and a small H^- solubility into MgF_2 rich materials. It is interesting to note that our results show that both H^- is dissolved into MgF_2 and F^- into MgH_2. Moreover, the smooth changes in the lattice parameters of $MgH_{2-x}F_x$ and MgH_yF_{2-y} suggests the existence of a broad range of fluorine solubility in magnesium hydride and of hydrogen in magnesium fluoride. Interchange of H^- and F^- ions has been found in other systems. Brice et al. reported the existence of a solution of stoichiometry $CaF_{2-x}H_x$ with $(0 < x \leq 1.24)$ prepared by heating CaF_2 and CaH_2 at 700 °C [26]. In this case both starting compounds have the CaF_2-type cubic symmetry. Messer et al. reported the interchange of H^- and F^- ions in the system LiH-LiF which presents the sodium chloride type crystal structure [27]. Also with the same crystalline structure, Majzoub et al. have observed F solubility into NaH [28]. Additionally, Saldan et al. have suggested the existence of a mixed $LiBH_{4-x}F_x$ phase [29]. On the other hand, DFT calculations made by Yin et al. have shown that F^- can substitute H^- in Na_3AlH_6 [30].

Hydrogen release from the as-milled materials

The decomposition of the as-milled materials has been studied by DSC, TG and TPD. Fig. 7 shows DSC curves of the 3,10 and 80 h-milled materials (intermediate milling times not shown for clarity). All curves show one endothermic event located between 200 and 300 °C that corresponds to MgH_2 or solid solutions decomposition. The materials milled 10 h or more show an additional endothermic peak around 400 °C associated with NbH dehydriding, as was verified by XRD patterns of samples extracted at intermediates temperatures. The presence of two endothermic events has also been reported in samples with 2 mol% of additive [7]. In the case of the 3 h-milled material, there are two additional exothermic events: a small one at $T = 72$ °C and a big one that starts around $T = 120$ °C and overlaps with the endothermic peak associated with MgH_2 decomposition. The first one can be attributed to MgF_2 formation from $MgNbF_7$ and MgH_2; the second one corresponds to reaction (2). We have shown that after 3 h of milling the reaction between MgH_2 and NbF_5 has not finished. According to Fig. 1, only 40% of NbF_5 has reacted at this milling time. The area of this second exothermic event is compatible with the value of the enthalpy associated with reaction (2) and the amount of remnant reactives. Remarkably, the solid solutions decomposition occurs 100 °C below the dehydriding temperature of MgH_2 without additive. Similar improvements have been reported for MgH_2 catalyzed with NbF_5 [3,5,7]. Besides, this kinetic improvement is reached after only 3 h in a low energy ball-mill, indicating that the products that give the catalytic effect are formed during the early milling stages. Additionally, we note that the DSC curve of the 80 h-milled material is slightly shifted towards higher temperatures, revealing that long milling times somewhat impair hydrogen desorption kinetics. The 3 h curve is a little shifted towards higher temperatures but this is an effect of the superposition of the dehydriding peak with the exothermic peak associated with MgF_2 formation. TG experiments (see Fig. 8 below) confirm that hydrogen release occurs at higher temperatures as milling time increases.

TG results are presented in Fig. 8. In agreement with DSC, samples with additive released hydrogen at a temperature approximately 100 °C below the decomposition temperature of the reference material. The registered mass losses are slightly below the theoretical H capacity of the material. This aspect will be discussed later. However, it is interesting to note that the magnitude of the mass changes allows us to discard a significant release of HF. The decomposition of the 10 and 80 h-milled materials occurs in two stages. The first one extends from 200–225 °C up to 275 °C and the second one begins at 275 °C without finishing at 450 °C, the maximum temperature reached in these experiments. The second regime is considerably slower than the first one, and releases more H_2 in the case of the materials milled longer times. This regime presents an almost linear temperature-dependence, that correspond in the DSC curves to the higher baselines observed after the main peak. A similar two-stage desorption in a MgH_2-4 mol% NbF_5 mixture has been observed by Sabitu et al. [16].

TPD experiments up to higher temperatures have been carried out on the 80 h-milled material. As a whole, the curve

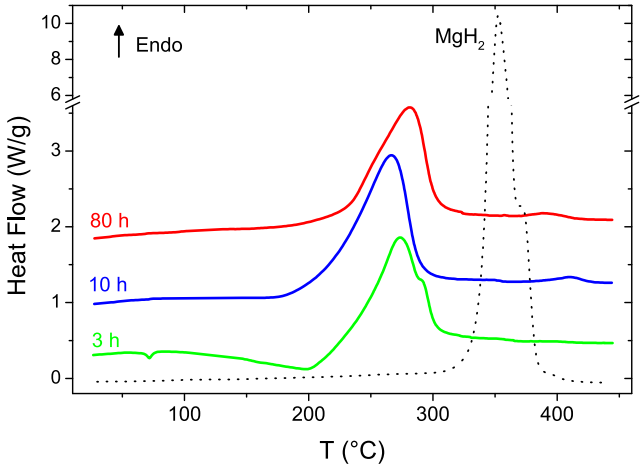

Fig. 7 – DSC of samples milled 3, 10 and 80 h. Results for a sample milled 80 h without additive is shown for comparison.

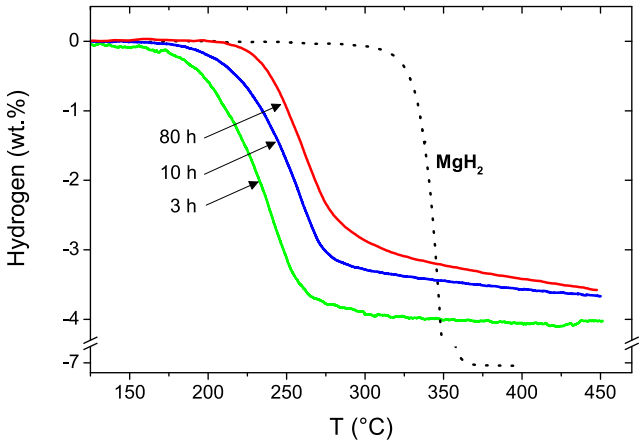

Fig. 8 – TG of samples milled 3, 10 and 80 h. Results for a sample milled 80 h without additive is shown for comparison.

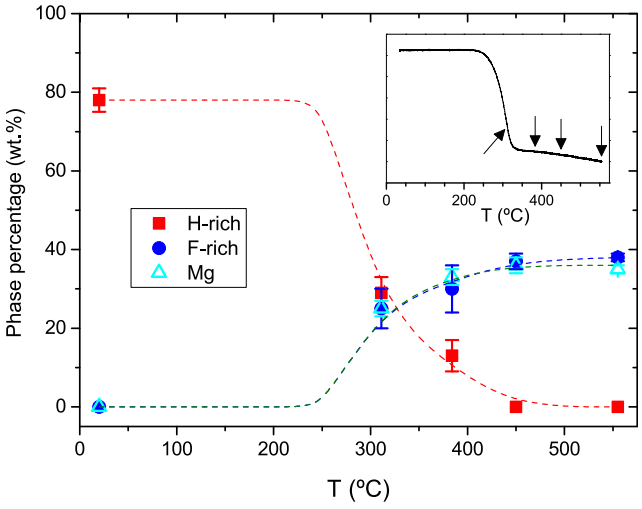

Fig. 9 – Amount of *Mg*, *H*-rich and *F*-rich solutions obtained from Rietveld refinement of XRD data of samples extracted at intermediate temperatures during the TPD experiment (dotted lines are a guide to the eye). The inset shows the TPD curve and the arrows indicate the extraction points.

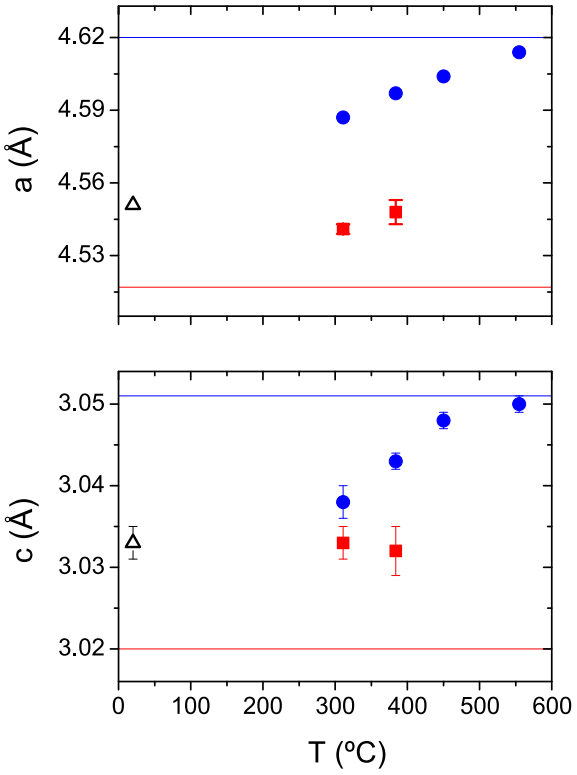

Fig. 10 – Lattice parameters of the *H*-rich (red squares) and *F*-rich (blue circles) solid solutions of samples extracted at intermediate temperatures during the TPD experiment. Open black triangles corresponds to the lattice parameters of the single solid solution of the 80 h-milled material. Red and blue lines are the lattice parameters of β-MgH_2 and MgF_2, respectively, reported in the PDF data. (For interpretation of the references to color in this figure legend, the reader is referred to the web version of this article.)

features are entirely compatible with DSC and TG results (inset of Fig. 9). To gain further insight in the desorption process some of these measurements have been interrupted at intermediate temperatures and the partially desorbed materials have been analyzed by XRD. The diffractograms show that two solid solutions ($MgH_{2-x}F_x$ and MgH_yF_{2-y}), *Mg*, β-*NbH*, and a small amount of *MgO* are present at temperatures below 450 °C. Above 450 °C the H-rich phase is no longer detected, and at 555 °C *Nb* is observed instead of β-*NbH*. The proportion of both solid solutions and *Mg* as a function of temperature, and the lattice parameters of the solid solutions obtained from Rietveld refinement of the data are presented in Figs. 9 and 10, respectively. It can be seen that after desorption begins around 250 °C the amount of $MgH_{2-x}F_x$ diminishes with temperature whereas the quantities of MgH_yF_{2-y} and *Mg* grow. The lattice parameters of the F-rich solution gradually move from the values of the as-milled material to those of MgF_2 as temperature increases, whereas the *a* and *c* values of the *H*-rich phase do not change with a clear tendency and remain close to those of the as-milled material. These results show that during desorption below 450 °C the *H*-rich solution releases H_2 and gives an *F*-enriched solution and *Mg* as products. Simultaneously, the *F*-rich solution also releases H_2 and becomes richer in F. At 450 °C and above only the F-rich solution releases H_2. Both desorption processes can be represented with different z values by the reaction:

$$MgH_{2-z}F_z \rightarrow \frac{z}{w}MgH_{2-w}F_w + \frac{w-z}{w}Mg + \frac{w-z}{w}H_2. \quad (4)$$

Note that this process involves solid solutions in a wide composition range. The observation of several intermediate values of lattice parameters for the *F*-rich solution during desorption supports this idea. A deep study of this, and the determination of the thermodynamic parameters of these solutions, will be the subject of a separate contribution.

The observation of two desorption regimes can be tentatively explained as follows. At the beginning of desorption, when the F^- concentration is below a threshold value, H_2 desorption is fast and the first desorption regime is observed. As the material becomes *F*-richer, H_2 desorption starts to be limited by fluorine diffusion, and the second desorption regime arises. A slower fluorine diffusion is expected because although *H* and *F* anions have similar sizes when interacting with *Mg*, they differ in mass in an order of magnitude. The argument was also proposed by Brice et al., who reported a lower anionic conductivity in fluorine rich solutions for the system CaH_2-CaF_2 [26]. The threshold value that separates both regimes can be estimated from the F^- occupancy of the Wyckoff 4*f* site. The proportion of F^- at 311 °C, in the middle of the first desorption regime is around 73%, and at 384 °C, at the beginning of the second regime, is near 79%. So the threshold value could be within this range. For comparison, the percolation threshold in a cubic lattice with a diffusing species and an immobile component partially occupying the diffusion sites is 70% [31].

To better understand the relationship between the amount of H_2 evolved and the composition of both solid solutions we

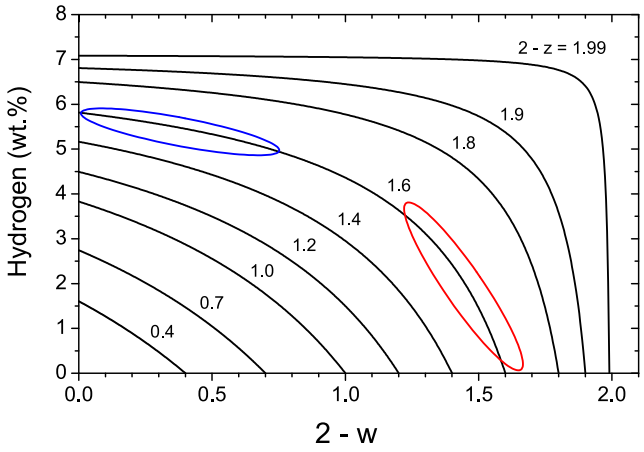

Fig. 11 – Amount of H_2 released following reaction (4) for different values of 2 – z as a function of 2 – w.

have calculated the theoretical amount of H_2 released following reaction (4) for different values of 2 – z as a function of 2 – w (Fig. 11). The shape of curves with higher 2 – z values shows that two different stages can be identified in the process described by reaction (4). Following the 2 – z = 1.6 curve we can see that at the beginning of the reaction a substantial amount of H_2 can be released with small compositional changes in the solution (zone marked in red in Fig. 11 (in the web version)), whereas once lower 2 – w values are reached, a small amount of H_2 is released with strong variations in composition (zone marked in blue in Fig. 11). This characteristic of reaction (4) is similar to the behavior observed in the TG and TPD experiments: a substantial amount of H_2 is released during the first desorption regime and a minor quantity during the second one.

Hydrogen absorption and desorption

Hydriding and dehydriding have also been studied by isothermal experiments in a Sievert-type apparatus. H_2 release from the as-milled material is slightly slower than desorption from a rehydrided sample (Fig. 12). After this second desorption, the material has shown very good repeatability. The additive significantly improves kinetics, in agreement with literature results [5,7,9,17]. In the absorption case, the sample milled 80 h with NbF_5 absorbs 2 wt.% in 200 s at T = 250 °C, whereas the material without additive takes half this value at the same time. Increasing the temperature up to T = 300 °C does not produce significant changes in hydrogen absorption in the material prepared with additive, only an increase in capacity. The absorption times are in the range reported for this type of material: between 1 and 5 min at T = 300 °C for samples with 1 or 2 mol% NbF_5 [7,11] and around 10 min at T = 250 and 300 °C [5]. In the desorption case, the samples with additive perform markedly better than the reference material. Whereas the milled MgH_2 takes nearly 2 h at T = 300 °C to be completely dehydrided (and practically does not desorb hydrogen at T = 250 °C), the material with NbF_5 can be decomposed within 1 min at T = 300 °C and after 7 min at T = 250 °C. These desorption times are shorter than the values reported for samples at 300 °C up to now: 30 min [9] for a

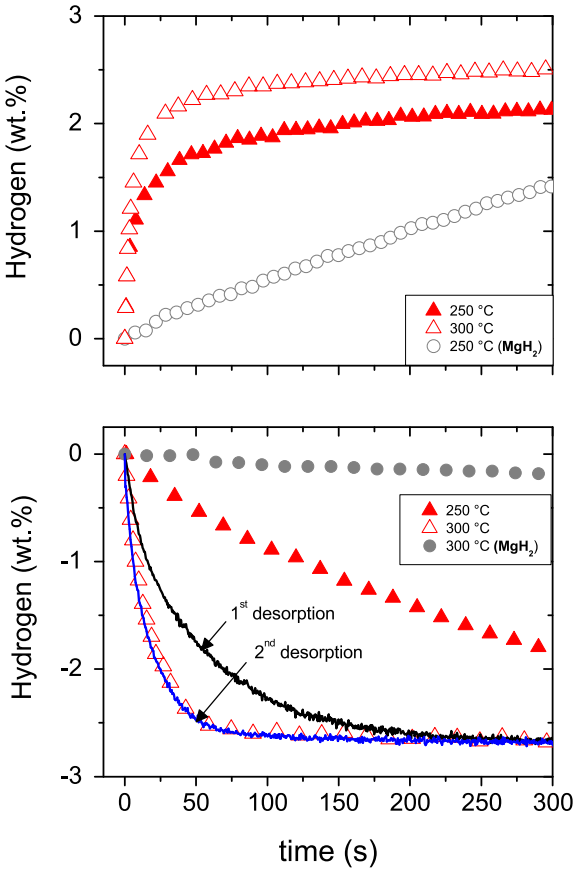

Fig. 12 – Isothermal hydriding and dehydriding curves of the 80 h-milled sample and the reference material. Absorption was done at 1000 kPa and desorption at 30 kPa. The first and second desorptions were measured at 300 °C.

sample with 2 mol% NbF_5, 20–30 min for samples with 5 wt.% [11] and 2 mol% [7] of additive, and 10 min for sample with 1 mol% NbF_5 [5]. At T = 250 °C, Recham [9] reported a desorption time of 40 min for a sample with 2 mol% NbF_5.

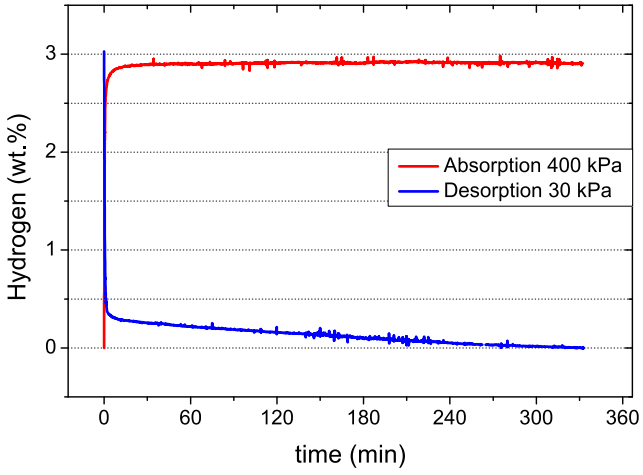

Fig. 13 – Isothermal hydriding and dehydriding curves of the 80 h-milled sample measured at T = 300 °C for longer time.

Probably our better desorption results are due to the higher proportion of additive.

Though the desorption process seems to have finished in Fig. 12, longer experiments have revealed that desorption continues at a much slower rate if the material is kept under dehydriding conditions (Fig. 13). The similarity with the desorption behavior of the as-milled material suggests that two desorption regimes could also take place in the cycled sample. On the contrary, absorption in this material takes place in a single and quick stage. This was expected, as F diffusion is not required to hydride Mg. An XRD measurement of the 80 h-milled material cycled three times and hydrided at 1000 kPa at $T = 300$ °C for 1600 s (Fig. 14) shows H-rich and F-rich solutions, α-NbH, and a small amount of unreacted Mg with their reflections slightly shifted towards the left. This last shift could be due to the presence of some F dissolved into it, as Mulder et al. suggested could take place in TiF_3-catalyzed MgH_2 [14]. However, a conclusive determination could not be done here. The observation of a H-rich solution instead of β-MgH_2 suggests that a complex process takes place during hydrogen absorption. If some F is effectively dissolved into Mg, this F could be kept within the structure when Mg takes up H and by this process produce the H-rich solution. Otherwise, if Mg does not contain F, MgH_2 would be formed from Mg and H_2, and after a few diffusive steps, it could take some F^- from the F-rich solution and produce the H-rich solution. Also, both processes could occur simultaneously. From our results we could not determine which one of these situations takes place. Undoubtedly, hydriding this material is a process in which possible compositional inhomogeneity and the dynamic characteristics of absorption and desorption are just a few factors that could contribute to a complex evolution. In any case, as a whole, the material behaves as a H-rich solution that reversibly releases and gets H_2.

Though the fact of taking up and releasing H_2 from a H-rich solution with a unit cell bigger than that of β-MgH_2 could lead to an enhanced diffusion process in this material, we can discard a significant contribution of this phenomenon to the faster H_2 absorption and desorption. In the desorption case the 3 h-milled material already presents a fast H_2 release, but after this milling time a minor amount of F^- is dissolved into MgH_2. In the absorption case, our hydriding rates are similar to those reported in the literature, but these last results correspond to a much lesser amount of F, and hence to a less enlarged unit cell. On the other hand, a possible effect of a F-rich solution should be considered. Mulder et al. [14] have suggested that the isostructural MgF_2 could act as a seeding crystal for MgH_2 during hydrogen absorption. In our case, this effect would be enhanced, as the inclusion of some H^- in the MgF_2 lattice reduces its cell size and thus improves the matching between the H-rich and F-rich solutions lattices. This phenomenon could also explain why transition metal fluorides are more effective than chlorides as additives, as $MgCl_2$ does not have the same crystallographic structure of β-MgH_2 and would not behave as an appropriate seeding crystal. However, the observed kinetic improvements cannot be attributed to the F-rich solution only. The evidence present in the literature shows that MgF_2 alone does not produce the same kinetic enhancements than those obtained with NbF_5 or other transition metal fluorides [19]. Although the additives distribution and the microstructure of the material are different if MgF_2 or a transition metal fluoride are added, it seems that the transition metal also contributes to the catalytic effect. Moreover, in several papers it has been proposed that the transition metal hydride plays the main catalytic role [5,8,32]. In the systematic study of Jin et al. analyzing various transition metal fluorides [4] they have found that the fluorides of transition metals that form hydrides are the ones that present the better kinetic improvements. In our materials we have confirmed by XRD that α-NbH is present in the cycled material both in the hydrided and dehydrided state. Hence, this compound and not Nb is the other phase present that could play a catalytic role, perhaps acting as a gateway for hydrogen transfer, as first proposed by Pelletier et al. [32]. However, it should be taken in mind that the hydriding and dehydriding processes in these materials are really complex, and a cooperative phenomenon of all the phases involved with a main α-NbH role is the most probable scenario.

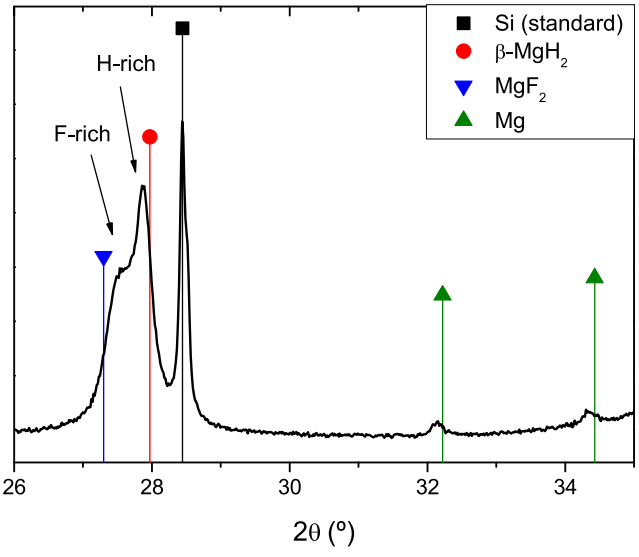

Fig. 14 – Diffractogram of a three-times-cycled sample after hydriding.

Conclusions

The main conclusions of this work are:

- Solid solutions in the system Mg–H–F have been found by milling MgH_2 and NbF_5. These compounds form H-rich and F-rich solid solutions with formulas $MgH_{2-x}F_x$ and MgH_yF_{2-y}, respectively. The amount of solute in each solution depends on milling time. After 40 h of milling both solutions merge into one with formula $MgH_{1.60}F_{0.40}$. The solutions have the same tetragonal $P4_2/mnm$ symmetry of MgH_2 and MgF_2, but with the Wyckoff position 4f randomly occupied by H^- or F^-. This solution does not decompose after being kept 90 h at 300 °C under 6000 kPa of H_2.
- The kinetics of hydrogen desorption from the synthesized material is greatly enhanced in comparison with MgH_2. The decomposition temperature in DSC or TG experiments are lowered by almost 100 °C, and 7 min are required to

dehydride the material in a volumetric device at $T = 250\,^{\circ}C$. Absorption kinetics are greatly enhanced as well. The material modified with NbF_5 takes up 2 wt.% in 200 s at $T = 250\,^{\circ}C$ whereas the material without additive only absorbs 1 wt.% in the same period.

- The desorption process in the as-milled and in the cycled material presents two stages. The last one is considerably slower than the first one, and is attributed to a desorption process controlled by F^- diffusion. H_2 absorption in the cycled material takes place in a single stage. XRD measurements show that the main *H*-containing phase in this material is a *H*-rich solution instead of MgH_2.
- An enhanced H^- diffusion in the *H*-rich solution due to the enlargement of the unit cell as a consequence of the F^- dissolved into the matrix could be discarded as an important contribution to the faster observed kinetics. The significant improvement in kinetics can be explained by a seeding crystal effect of the *F*-rich solution and a gateway effect of niobium hydride.

Acknowledgments

This work was partially supported by grants from Universidad Nacional de Cuyo, FONCyT PAE (PICT N◦ 133), and CONICET (PIP 112 201101 00524).

REFERENCES

[1] Jain I, Lal C, Jain A. Hydrogen storage in *Mg*: a most promising material. Int J Hydrogen Energy 2010;35(10):5133–44. http://dx.doi.org/10.1016/j.ijhydene.2009.08.088.

[2] Huot J, Ravnsbæk D, Zhang J, Cuevas F, Latroche M, Jensen T. Mechanochemical synthesis of hydrogen storage materials. Prog Mater Sci 2013;58(1):30–75. http://dx.doi.org/10.1016/j.pmatsci.2012.07.001.

[3] Malka IE, Czujko T, Bystrzycki J. Catalytic effect of halide additives ball milled with magnesium hydride. Int J Hydrogen Energy 2010;35(4):1706–12. http://dx.doi.org/10.1016/j.ijhydene.2009.12.024.

[4] Jin S-A, Shim J-H, Cho YW, Yi K-W. Dehydrogenation and hydrogenation characteristics of MgH_2 with transition metal fluorides. J Power Sources 2007;172(2):859–62. http://dx.doi.org/10.1016/j.jpowsour.2007.04.090.

[5] Jin S-A, Shim J-H, Ahn J-P, Cho YW, Yi K-W. Improvement in hydrogen sorption kinetics of MgH_2 with Nb hydride catalyst. Acta Mater 2007;55(15):5073–9. http://dx.doi.org/10.1016/j.actamat.2007.05.029.

[6] Kwak Y-J, Song J, Mumm D-R. Improvement of hydrogen storage properties of *Mg* by addition of NbF_5 via mechanical milling under H_2. Kor J Mater Res 2013;23(10):562–7. http://dx.doi.org/10.3740/MRSK.2013.23.10.562.

[7] Luo Y, Wang P, Ma L-P, Cheng H-M. Hydrogen sorption kinetics of MgH_2 catalyzed with NbF_5. J Alloys Compd 2008;453(1–2):138–42. http://dx.doi.org/10.1016/j.jallcom.2006.11.113.

[8] Ma L-P, Wang P, Cheng H-M. Hydrogen sorption kinetics of MgH_2 catalyzed with titanium compounds. Int J Hydrogen Energy 2010;35(7):3046–50. http://dx.doi.org/10.1016/j.ijhydene.2009.07.014. 2008 International Hydrogen Forum (HyForum2008).

[9] Recham N, Bhat V, Kandavel M, Aymard L, Tarascon J-M, Rougier A. Reduction of hydrogen desorption temperature of ball-milled MgH_2 by NbF_5 addition. J Alloys Compd 2008;464(12):377–82. http://dx.doi.org/10.1016/j.jallcom.2007.09.130.

[10] Leiva D-R, Ishikawa T-T, Miraglia S, Fruchart D, Botta W-J. Reactive milling of magnesium under hydrogen using transition metals and their fluorides as additives. Solid State Phenom 2013;194:232–6. http://dx.doi.org/10.4028/www.scientific.net/SSP.194.232.

[11] Luo Y, Wang P, Ma L-P, Cheng H-M. Enhanced hydrogen storage properties of MgH_2 co-catalyzed with NbF_5 and single-walled carbon nanotubes. Scr Mater 2007;56(9):765–8. http://dx.doi.org/10.1016/j.scriptamat.2007.01.016.

[12] Xie L, Liu Y, Wang Y, Zheng J, Li X. Superior hydrogen storage kinetics of MgH_2 nanoparticles doped with TiF_3. Acta Mater 2007;55(13):4585–91. http://dx.doi.org/10.1016/j.actamat.2007.04.020.

[13] Ma L-P, Wang P, Cheng H-M. Improving hydrogen sorption kinetics of MgH_2 by mechanical milling with TiF_3. J Alloys Compd 2007;432(1–2):L1–4. http://dx.doi.org/10.1016/j.jallcom.2006.05.103.

[14] Mulder FM, Singh S, Bolhuis S, Eijt SWH. Extended solubility limits and nanograin refinement in *Ti/Zr* fluoride-catalyzed MgH_2. J Phys Chem C 2012;116(2):2001–12. http://dx.doi.org/10.1021/jp204121c.

[15] Kim JW, Ahn J-P, Jin S-A, Lee SH, Chung H-S, Shim J-H, et al. Microstructural evolution of NbF_5-doped MgH_2 exhibiting fast hydrogen sorption kinetics. J Power Sources 2008;178(1):373–8. http://dx.doi.org/10.1016/j.jpowsour.2007.12.005.

[16] Sabitu ST, Goudy AJ. Dehydrogenation kinetics and modeling studies of MgH_2 enhanced by NbF_5 catalyst using constant pressure thermodynamic forces. Int J Hydrogen Energy 2012;37(17):12301–6. http://dx.doi.org/10.1016/j.ijhydene.2012.06.039. 12th CHEC.

[17] Malka IE, Pisarek M, Czujko T, Bystrzycki J. A study of the ZrF_4, NbF_5, TaF_5, and $TiCl_3$ influences on the MgH_2 sorption properties. Int J Hydrogen Energy 2011;36(20):12909–17. http://dx.doi.org/10.1016/j.ijhydene.2011.07.020.

[18] Ivanov E, Konstanchuk I, Bokhonov B, Boldyrev V. Hydrogen interaction with mechanically alloyed magnesium-salt composite materials. J Alloys Compd 2003;359(1–2):320–5. http://dx.doi.org/10.1016/S0925-8388(03) 00297–4.

[19] Ma L-P, Kang X-D, Dai H-B, Liang Y, Fang Z-Z, Wang P-J, et al. Superior catalytic effect of TiF_3 over $TiCl_3$ in improving the hydrogen sorption kinetics of MgH_2: catalytic role of fluorine anion. Acta Mater 2009;57(7):2250–8. http://dx.doi.org/10.1016/j.actamat.2009.01.025.

[20] Rodríguez-Carvajal J. Recent advances in magnetic structure determination by neutron powder diffraction. Phys B – Phys Condens Matter 1993;192(1–2):55–69. http://dx.doi.org/10.1016/0921-4526(93)90108-I.

[21] Meyer G, Rodríguez D, Castro F, Fernández G. Automatic device for precise characterization of hydride forming materials. In: 11th World hydrogen energy conference, vol. 2; 1996. p. 1293. Stuttgart.

[22] Manchester FE. Phase diagrams of binary hydrogen alloys. Monograph series on alloy phase diagrams, vol. 13. Ohio: ASM International; 2000.

[23] Kubaschewski O, Alcock C, Spencer P. Materials thermochemistry. 6th ed. Oxford: Pergamon Press; 1993.

[24] Suryanarayana C. Mechanical alloying and milling. Prog Mater Sci 2001;46(12):1–184. http://dx.doi.org/10.1016/S0079-6425(99)00010-9.

[25] Baricco M, Palumbo M, Pinatel E, Corno M, Ugliengo P. Thermodynamic database for hydrogen storage materials.

Adv Sci Technol 2010;72:213–8. http://dx.doi.org/10.4028/www.scientific.net/AST.72.213.

[26] Brice J-F, Courtois A, Aubry J. Preparation de la solution solide hydrurofluoree $CaF_{2-x}H_x$ (0<x<1.24) etude structurale par diffraction des rayons x et par diffraction des neutrons. J Solid State Chem 1978;24(34):381–7. http://dx.doi.org/10.1016/0022-4596(78)90030-0.

[27] Messer CE, Mellor J. The system lithium hydride – lithium fluoride. J Phys Chem 1960;64(4):503–5. http://dx.doi.org/10.1021/j100833a507.

[28] Majzoub E, Herberg J, Stumpf R, Spangler S, Maxwell R. XRD and NMR investigation of *Ti*-compound formation in solution-doping of sodium aluminum hydrides: solubility of *Ti* in $NaAlH_4$ crystals grown in THF. J Alloys Compd 2005;394(12):265–70. http://dx.doi.org/10.1016/j.jallcom.2004.10.056.

[29] Saldan I, Ramallo-López JM, Requejo FG, Suarez-Alcantara K, Von Colbe JB, Avila J. NEXAFS study of $2LiF-MgB_2$ composite. Int J Hydrogen Energy 2012;37(13):10236–9. http://dx.doi.org/10.1016/j.ijhydene.2012.04.010.

[30] Yin L-C, Wang P, Kang X-D, Sun C-H, Cheng H-M. Functional anion concept: effect of fluorine anion on hydrogen storage of sodium alanate. Phys Chem Chem Phys 2007;9:1499–502. http://dx.doi.org/10.1039/B610257C.

[31] Benes NE, Bouwmeester HJ, Verweij H. Multi-component lattice gas diffusion. Chem Eng Sci 2002;57(14):2673–8. http://dx.doi.org/10.1016/S0009-2509(02)00154-9.

[32] Pelletier JF, Huot J, Sutton M, Schulz R, Sandy AR, Lurio LB, et al. Hydrogen desorption mechanism in MgH_2-*Nb* nanocomposites. Phys Rev B 2001;63:052103. http://dx.doi.org/10.1103/PhysRevB.63.052103.